

J Mater Sci (2014) 49:3936–3942
DOI 10.1007/s10853-013-7958-5

INTERGRANULAR AND INTERPHASE BOUNDARIES

Twist, tilt, and symmetric grain boundaries in hexagonal materials

Krzysztof Glowinski · Adam Morawiec

Received: 21 September 2013 / Accepted: 10 December 2013 / Published online: 24 December 2013
© The Author(s) 2013. This article is published with open access at Springerlink.com

Abstract Grain boundaries of characteristic geometry, e.g., twist, tilt, and symmetric boundaries are often used as reference boundaries in analyses of boundary networks in polycrystalline materials. This article deals with the issue of proper identification of characteristic boundaries in the case of materials with hexagonal D_{6h} symmetry. To identify all boundaries of characteristic types, both analytical calculations and numerical searches are used. The first approach provides exact parameters of the characteristic boundaries, whereas the second one gives boundaries which can be classified as characteristic if some tolerance is allowed. In both methods, all symmetrically equivalent boundary representations are taken into consideration. The obtained sets of twist, tilt, symmetric, and 180° -tilt boundaries are presented in the form of two-dimensional maps containing stereographic projections of the corresponding boundary plane normals for selected grain misorientations. These diagrams facilitate interpretation of experimental distributions of grain boundaries; with the representation used, they can be directly linked to experimental distributions. Examples of such diagrams for lattice parameter ratios c/a of $\sqrt{5/2}$ and $\sqrt{20/21}$ are presented. They are compared to example boundary distributions in Ti alloy and distributions of WC/WC boundaries in WC–Co composites available in the literature.

Introduction

A wide range of properties of polycrystalline materials is influenced by intergranular boundaries. The most basic attribute of a boundary is its “macroscopic” geometry, which can be described by a misorientation between neighboring grains and boundary plane indices, i.e., by five independent parameters [1]. A thorough understanding of macroscopic features of boundaries is essential for more comprehensive boundary studies at the atomic scale. Thanks to recent advances in development of both destructive (e.g., [2]) and nondestructive (e.g., [3]) three-dimensional techniques of microstructure imaging, the five macroscopic parameters of significant numbers of boundaries are experimentally accessible. The large sizes of boundary data sets open new possibilities for carrying out statistical analyses of boundary networks. In particular, distributions of grain boundaries with respect to their macroscopic parameters are studied (e.g., [4–6]). These distributions indicate which boundary geometries are preferred, and which are underrepresented. The question arises whether maxima in the distributions correspond to boundaries of special geometries, e.g., to twist, tilt, or symmetric boundaries. To answer it, the boundaries having characteristic geometries need to be properly identified. In the presence of crystal symmetries, every geometric configuration may have multiple equivalent representations; it is crucial to take them all into consideration to recognize boundary types correctly.

All twist and tilt boundaries of low-Sigma misorientations for the cubic O_h symmetry were cataloged in [7]; for each of these misorientations, the catalogs of twist and tilt boundaries were presented in the form of two-dimensional maps containing stereographic projections of the corresponding boundary plane normals. With this

K. Glowinski (✉) · A. Morawiec
Institute of Metallurgy and Materials Science, Polish Academy of Sciences, Reymonta 25, 30-059 Kraków, Poland
e-mail: kglowinski@gmail.com

A. Morawiec
e-mail: nmmorawi@cyf-kr.edu.pl

representation, the obtained diagrams can be directly linked to the experimental distributions, which are usually displayed in a similar way, i.e., as functions of boundary planes for fixed misorientations. These maps were afterward completed with symmetric and 180°-tilt boundaries in [8].

Since distributions of boundaries in hexagonal materials are also of interest (e.g., [5, 6]), the purpose of this article is to extend the previous studies and to provide analogous patterns for materials of hexagonal D_{6h} symmetry. Differently than in the cubic case, the resulting figures depend on lattice parameters. We consider the cases of $c/a = \sqrt{5/2}$ and $c/a = \sqrt{20/21}$. These ratios correspond, respectively, to α -phase titanium and tungsten carbide. Diagrams containing all twist, tilt, symmetric, and 180°-tilt boundaries for selected misorientations are presented below. The diagrams have been obtained using two complementary approaches: analytical and numerical. The first method allows for immediate determination of exact locations of boundaries of characteristic geometry. However, in practice, experimental errors must be taken into account. The second approach provides all boundaries that satisfy type-defining conditions with assumed tolerance thresholds; it utilizes certain parameters introduced recently [9] to approximate the distances (defined in the space of boundary parameters [10–12]) to the nearest twist, tilt, symmetric, and 180°-tilt boundaries. The costs of computing these parameters are low, and therefore, the diagrams are obtained more effectively compared to the time-consuming accurate calculation of the distances used in [7].

To demonstrate the usefulness of our patterns and to indicate issues related to interpretation of the experimental distributions, some of the obtained diagrams are compared to example sections through experimental distributions of grain boundaries in Ti alloy published in [6] and WC/WC boundaries in WC–Co composites presented in [5]; the peaks reported in the sections through the distribution of WC/WC boundaries are characterized in a systematic way.

Methods

Analytical calculations

In the case of D_{6h} symmetry, geometry of a boundary is fully described by a misorientation M and Miller-Bravais indices $(h_1 \ k_1 \ i_1 \ l_1)$ of the boundary plane expressed in the reference frame of the first grain [11]. The indices of that plane given in the frame attached to the second grain are $(h_2 \ k_2 \ i_2 \ l_2) = M^{-1} \circ (\bar{h}_1 \ \bar{k}_1 \ \bar{i}_1 \ \bar{l}_1)$, where the sign “ \circ ” denotes a rotation of a crystallographic plane. The same boundary can also be represented by $(h'_1 \ k'_1 \ i'_1 \ l'_1) = C_1 \circ (h_1 \ k_1 \ i_1 \ l_1)$, the

corresponding $(h'_2 \ k'_2 \ i'_2 \ l'_2) = C_2 \circ (h_2 \ k_2 \ i_2 \ l_2)$ with C_1 and C_2 being proper symmetry rotations of the considered point group applied to the first and second grains, respectively, and by equivalent misorientation $M' = C_1 \circ M \circ C_2^{-1}$ (here, “ \circ ” stands for compositions of rotations). Due to inversion symmetry, the representation by M and $(h_1 \ k_1 \ i_1 \ l_1)$ is equivalent to that by M and $(\bar{h}_1 \ \bar{k}_1 \ \bar{i}_1 \ \bar{l}_1)$. Additionally, for homo-phase boundaries, grain exchange symmetry implies that also the pair M^{-1} and $(h_2 \ k_2 \ i_2 \ l_2)$ describes the same boundary. Hence, for D_{6h} symmetry, there are up to $2 \times 2 \times 12 \times 12$ different equivalent grain boundary representations in the complete domain of the macroscopic parameters.

A boundary is referred to as a twist boundary if it has a representation with the misorientation axis perpendicular to the boundary plane, while for a tilt boundary, there exists a description with the axis lying in that plane. Symmetric boundaries can also be represented as 180°-twist boundaries; 180°-tilt boundaries are sometimes called improperly quasi-symmetric [13].

Grain boundaries will not be classified correctly unless equivalent representations are processed. It is not enough to limit the analysis to representations with *disorientations*, because many of the characteristic boundaries will be overlooked. For instance, a boundary in a material with $c/a \approx \sqrt{5/2}$ described by the $\Sigma 11b$ misorientation [14], i.e., 84.78° rotation about the $[2\bar{1}\bar{1}0]$ axis (denoted by $84.78^\circ/[2\bar{1}\bar{1}0]$), and the $(0\bar{1}12)$ plane is visibly a tilt boundary, but its 180°-twist and 180°-tilt characters are not directly apparent. However, this boundary can also be represented by the $180^\circ/[01\bar{1}\bar{1}]$ misorientation and $(0\bar{1}12)$ plane; thus, the boundary is indeed a 180°-tilt. Other equivalent parameters of this boundary are the $180^\circ/[05\bar{5}\bar{6}]$ misorientation and $(01\bar{1}2)$ plane; since the normal to the $(01\bar{1}2)$ boundary plane is $[05\bar{5}\bar{6}]$, the boundary has also a twist character.

The simplest algorithm for finding all boundaries of characteristic geometry is based on analytical derivations. First, one applies symmetry transformations C_1 and C_2 to a fixed misorientation M to get its equivalent representations M' . Then, based on the aforementioned type definitions, all planes of characteristic boundaries can be determined from the corresponding misorientation axes. Finally, by transforming the indices of these planes to the initial reference frame using inverse transformations C_1^{-1} and C_2^{-1} , one obtains the boundary normals to be included in a diagram. For instance, application of the transformations $C_1 = 180^\circ/[\bar{1}2\bar{1}0]$ and $C_2 = \text{identity}$ to the misorientation $M = 84.78^\circ/[2\bar{1}\bar{1}0]$ ($\Sigma 11b$) gives $M' = 180^\circ/[05\bar{5}\bar{6}]$. For this equivalent misorientation, boundaries with the planes $(01\bar{1}2)$ and $(0\bar{1}12)$ (with the normals $[05\bar{5}\bar{6}]$ and $[05\bar{5}\bar{6}]$, respectively) have explicit twist characters, and there is a

zone of planes parallel to the misorientation axis, i.e., corresponding explicitly to tilts. Since the misorientation is a half-turn, these twist and tilt boundaries are also symmetric and 180° -tilt boundaries, respectively. The indices of these planes need to be transformed to the initial reference frame, e.g., $C_1^{-1} \circ (01\bar{1}2) = (0\bar{1}12)$. Proceeding in an analogous manner with all misorientation representations, one finds all boundaries of characteristic geometry.

Numerical searches

Measured boundary parameters are affected by the experimental errors. The resolution for determination of boundary plane inclinations is relatively poor. For an apparatus combining electron backscatter diffraction and serial sectioning, it has been estimated to be about 7.5° [4]. Hence, it is difficult to match the measured parameters to the definitions of characteristic boundary types. Therefore, relying on patterns containing only exact locations of the boundaries of characteristic geometry (without any tolerance) is insufficient for interpretation of the boundary distributions.

With error-affected data, it is more suitable to identify boundary types using metric functions defined in the boundary space: if the distance from a given boundary to the nearest twist, tilt, or symmetric boundary is below an assumed threshold, then the boundary is classified as near-twist, near-tilt, or near-symmetric, respectively.

The distributions of these distances for fixed misorientations and varying boundary planes (displayed as two-dimensional contour graphs on stereographic projections, cf. [7]) may serve as patterns useful in analyses of grain boundary distributions. The patterns of this kind have the advantage in taking into account experimental uncertainties: the zero values clearly correspond to pure-twist, pure-tilt, or pure-symmetric boundaries, and the isolines corresponding to assumed tolerance thresholds surround all near-twist, near-tilt, or near-symmetric boundaries of given misorientations.

To obtain detailed diagrams for fixed misorientations, the values of the distances need to be probed at densely distributed boundary normals. Since calculation of the distances involves complex numerical algorithms [7], the times needed for obtaining the maps become long. This difficulty is circumvented by substituting the properly defined distances to the nearest twist, tilt, symmetric, and 180° -tilt boundaries by recently suggested approximating parameters [9]. These parameters are strongly correlated with the corresponding distances, so they provide similar characteristics of a given boundary, and they can be computed significantly faster than the distances. The times needed for computing the approximated maps are about three orders of magnitude shorter than those for the maps with the accurate distances.

Diagrams with characteristic boundaries

Example diagrams obtained using the analytical method for the c/a ratio at $\sqrt{5}/2$ and the $\Sigma 11b$ and $\Sigma 19a$ ($65.10^\circ/[10, \bar{5}, \bar{5}, 3]$) misorientations are presented in Fig. 1a, b. In these maps, twist boundaries and zones of tilt boundaries are represented by, respectively, points and lines. Symmetric boundaries being particular twist boundaries have less degrees of freedom, and in consequence, they occur less frequently than twists; similarly, 180° -tilts are less frequent than tilts (cf. [15]). E.g., for the $\Sigma 19a$ misorientation (Fig. 1b), among ten distinct twist boundaries and the ten corresponding tilt zones, there is only one symmetric boundary and one 180° -tilt zone.

Using the diagrams, one can identify boundaries with characteristic geometries. By this, we mean boundaries lying at the intersections of multiple tilt zones and boundaries ascribed to more than one type, e.g., $\Sigma 11b$ boundaries with $(1\bar{1}12)$ and $(03\bar{3}5)$ planes (Fig. 1a). Boundaries with multiple tilt axes must be two-dimensionally periodic; such ordered structures may have uncommon properties, especially if the tilt axes are low-index, i.e., if the periodically repeated cell is small. Boundaries being simultaneously of more than one type can be expected to have specific geometries, and therefore, they may also have special properties.

Example diagrams computed using the numerical approach, that is, the distributions of the approximated distances to the nearest characteristic boundaries for $c/a = \sqrt{20/21}$ and for the $90^\circ/[10\bar{1}0]$ and $30^\circ/[0001]$ misorientations are plotted in Figs. 2 and 3. For a given tolerance threshold, near-twist and near-tilt boundaries are represented by spots and bands, respectively. The figures are compared to the sections through experimental distribution of WC/WC grain boundaries in WC–Co composites described in [5].

Discussion

Similarly to the cubic case, the diagrams obtained for hexagonal symmetry reveal a variety of boundaries of characteristic geometry. Depending on the misorientation, the diagrams may exhibit some symmetries (cf. [16]), and not all of the identified characteristic boundaries correspond to macroscopically different configurations. There are groups of twist and tilt boundaries the planes of which belong to the same plane families. The symmetries in the boundary-plane distributions for a given misorientation follow from analysis of equivalent boundary representations analogous to that in the example in “Analytical

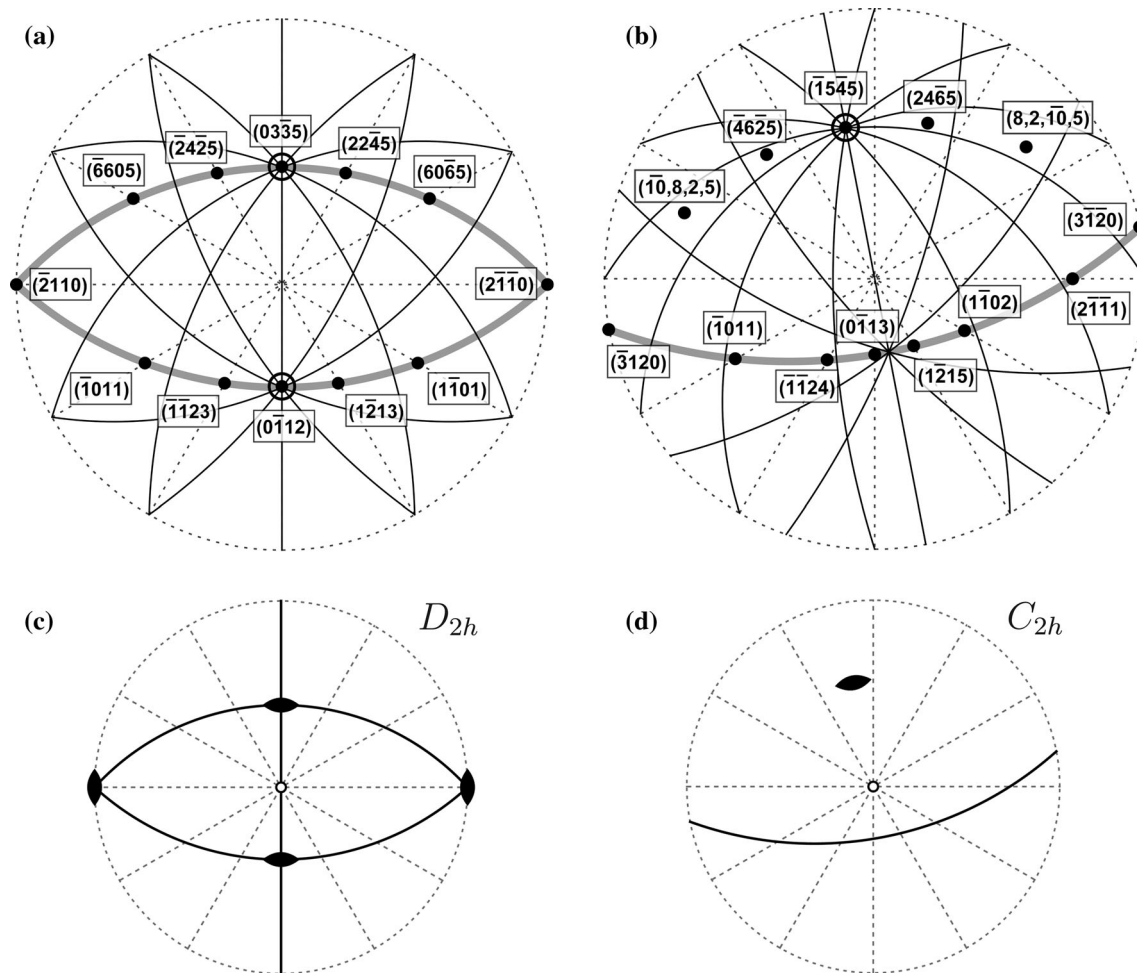


Fig. 1 Stereographic projections of poles of boundary planes corresponding to twist (*points*), tilt (*thin lines*), symmetric (*circles*), and 180°-tilt (*thick lines*) grain boundaries of the $\Sigma 11b$ (a) and $\Sigma 19a$

(b) misorientations and for $c/a = \sqrt{5}/2$; symmetries of boundary-plane distributions for these misorientations are shown in (c) and (d), respectively

calculations” section. The symmetries for the considered misorientations are shown in Figs. 1c, d, 2b, 3b.

The diagrams in Fig. 1 can be directly used to characterize the extrema occurring in the experimental distributions of boundaries in the Ti alloy presented in [6]. Let us focus on the diagram for the $\Sigma 19a$ misorientation (Fig. 1b) corresponding to the section through the experimental distribution (Fig. 4 of [6]). The peaks visible in that section were interpreted as corresponding to the $(4\bar{1}30)$ and $(\bar{4}130)$ boundary planes. With the tolerance of $<3^\circ$, the $\{4\bar{1}30\}$ planes are indistinguishable from the $\{3\bar{1}20\}$ planes. Thus, the observed peaks can be interpreted as special boundaries being simultaneously twists and 180°-tilts.

To demonstrate a possible scheme of interpretation of grain boundary distributions using numerically obtained patterns, we will characterize the peaks of the distribution of WC/WC boundaries in WC–Co composites. Let us consider each of the three sections through the distribution shown in Fig. 8 of [5].

- The section for the $90^\circ/[10\bar{1}0]$ misorientation (see Fig. 2) contains two strong peaks at the $(10\bar{1}0)$ and $(\bar{1}010)$ poles. These are directly related to pure-twist boundaries. With our maps, these two configurations are also recognized as double 180°-tilts. The distances of the peaks to symmetric boundaries are very large.
- In the case of the $30^\circ/[0001]$ misorientation (see Fig. 3), there is a maximum for the (0001) plane. These are the twist boundaries. The (0001) plane is also located at the intersection of six 180°-tilt zones. Elevated values of the distribution occurred also at the prismatic positions $(10\bar{1}0)$, $(11\bar{2}0)$. These are tilts, but they are neither twist nor symmetric nor 180°-tilt boundaries.
- In the distribution of boundary planes for the $90^\circ/[\bar{2}110]$ misorientation, there are peaks at the (0001) , $(1\bar{1}00)$, and $(\bar{1}100)$ poles. The distributions of the distances corresponding to this misorientation are almost identical to those for the $90^\circ/[10\bar{1}0]$ misorientation with the only

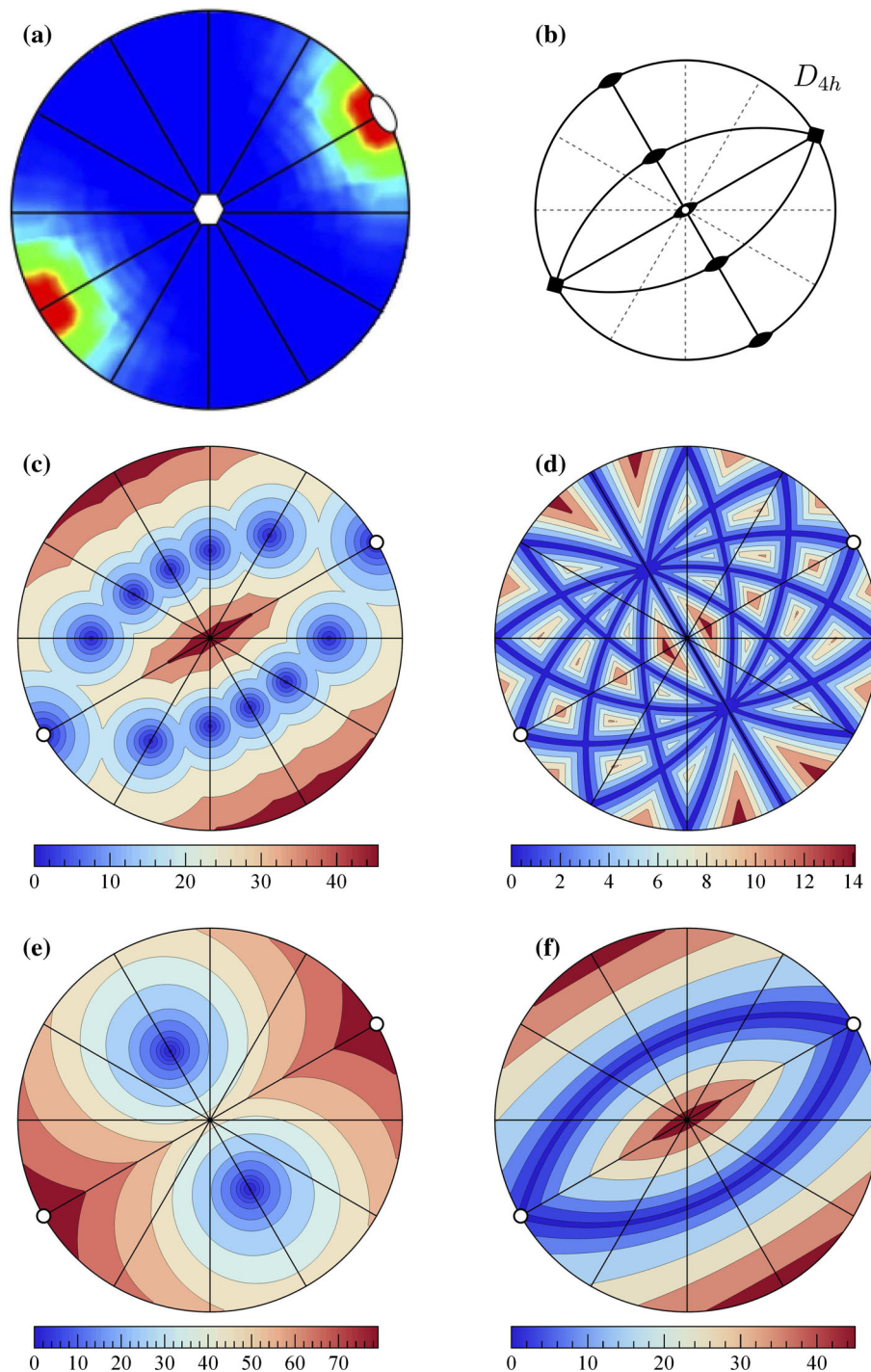


Fig. 2 Experimental distribution of planes of WC/WC boundaries for the $90^\circ/[10\bar{1}0]$ misorientation (a) reprinted from [5], with permission from John Wiley & Sons; its symmetries are shown in (b). The corresponding distributions (for $c/a = \sqrt{20/21}$) of the approximated

difference that they are rotated clockwise by 30° (therefore, only the latter are shown). The peak for the (0001) plane corresponds to a boundary with a single tilt axis. The other two maxima lie on the intersections of two tilt zones.

distances (in degrees) to the nearest twist (c), tilt (d), symmetric (e), and 180° -tilt (f) boundaries. The distributions are given as functions of boundary plane normals and plotted on stereographic projections. Locations of the peaks visible in (a) are marked in (c–f) with *white disks*

All these overrepresented boundaries have at least one tilt axis. Interestingly, none of them can be classified as symmetric. The two highest peaks are interpreted as twist boundaries located at the intersections of 180° -tilt zones. The interpretations of all the maxima are collected in Table 1.

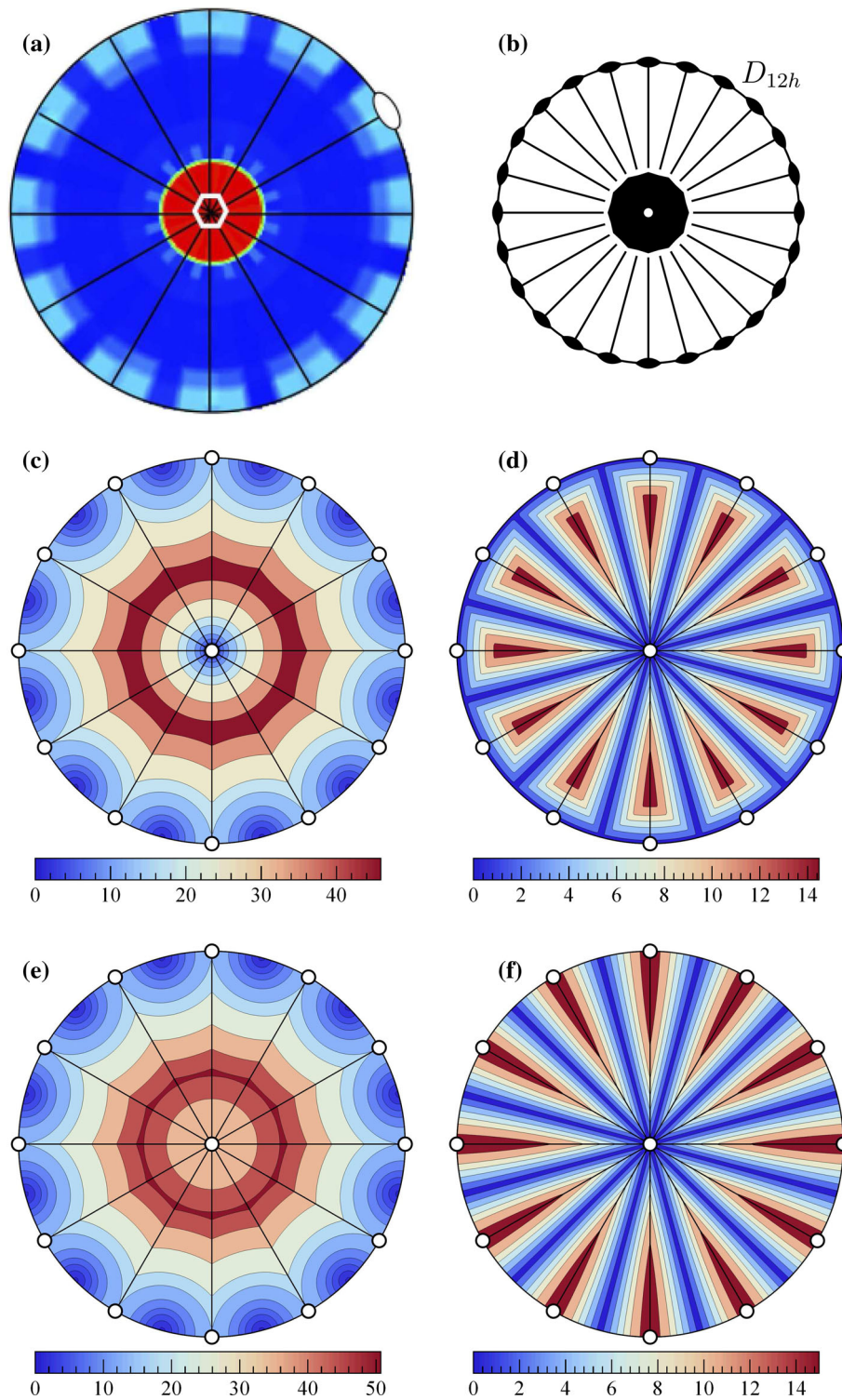


Fig. 3 Section through experimental distribution of WC/WC boundaries for the $30^\circ/[0001]$ misorientation (a) reprinted from [5], with permission from John Wiley & Sons; its symmetries are shown in (b). The related distributions (for $c/a = \sqrt{20/21}$) of the approximated distances (in degrees) to the nearest twist (c), tilt (d), symmetric (e),

and 180° -tilt (f) boundaries. The distributions are given as functions of boundary planes and are displayed on stereographic projections. Locations of the peaks visible in (a) are marked in (c–f) with *white disks*

Table 1 Characterization of the peaks in the distribution of WC/WC boundaries in a WC–Co composite

Misorientation	Plane	Peak height	Twist	Tilt	Symmetric	180°-tilt
90°/[10 $\bar{1}$ 0]	(10 $\bar{1}$ 0)	148	•	•(2)	–	•(2)
30°/[0001]	(0001)	18	•	•(6)	–	•(6)
	(10 $\bar{1}$ 0), (11 $\bar{2}$ 0)	5	–	•	–	–
90°/[$\bar{2}$ 110]	(0001)	8	–	•	–	–
	(1 $\bar{1}$ 00)	8	–	•(2)	–	–

The parameters and heights of the peaks (expressed as multiples of random distribution) are cited after [5]. Peaks identified as corresponding to a given boundary type are marked by the symbol “•”. For peaks located at the intersections of tilt zones, the numbers of zones are added in parentheses

Final remarks

Geometrically characteristic boundaries (i.e., twist, tilt, symmetric, and 180°-tilt boundaries) have been identified for selected misorientations between crystals of hexagonal holohedral symmetry with c/a ratios equal to $\sqrt{5/2}$ and $\sqrt{20/21}$. The obtained sets of boundaries with characteristic geometry for given misorientations have been presented in the form of diagrams containing stereographic projections of the poles of boundary planes. These diagrams are helpful in interpretation of the experimentally obtained grain boundary distributions. As an example, the peaks occurring in the distribution of WC/WC boundaries of [5] have been systematically characterized. In the distribution of WC/WC boundaries in WC–Co composites, all the reported maxima happen to correspond to either single- or multiple-tilt boundaries, and their geometries are far from symmetric geometry. The two highest peaks are also identified as special boundaries being twist boundaries located at the intersections of multiple 180°-tilt zones.

Grain boundaries are extensively studied using various techniques at different length scales. We believe that more detailed interpretation of boundary distributions may provide important hints for further investigations of both individual boundary types and quantitative studies of boundary networks. This work is focused on hexagonal materials, but the described methods can be applied to boundaries between crystals with other holohedral symmetries.

Acknowledgements The work of K.G. was supported by the European Union under the European Social Fund within Project No. POKL.04.01.00-00-004/10.

Open Access This article is distributed under the terms of the Creative Commons Attribution License which permits any use, distribution, and reproduction in any medium, provided the original author(s) and the source are credited.

References

- Goux C (1974) Structure of joined grains-crystallographic consideration and methods of structure estimation. *Can Metall Quart* 13:9–31
- Groeber MA, Haley BK, Uchic MD, Dimiduk DM, Ghosh S (2006) 3D reconstruction and characterization of polycrystalline microstructures using a FIB–SEM system. *Mater Charact* 57:259–273
- Poulsen HF (2012) An introduction to three-dimensional X-ray diffraction microscopy. *J Appl Cryst* 45:1084–1097
- Saylor DM, Morawiec A, Rohrer GS (2003) Distribution of grain boundaries in magnesia as a function of five macroscopic parameters. *Acta Mater* 51:3663–3674
- Kim C-S, Massa TR, Rohrer GS (2008) Interface character distributions in WC–Co composites. *J Am Ceram Soc* 91:996–1001
- Randle V, Rohrer GS, Hu Y (2008) Five-parameter grain boundary analysis of a titanium alloy before and after low-temperature annealing. *Scripta Mater* 58:183–186
- Morawiec A (2011) Low-Sigma twist and tilt grain boundaries in cubic materials. *J Appl Cryst* 44:1152–1156
- Glowinski K, Morawiec A (2012) A toolbox for geometric grain boundary characterization. In: De Graef M, Poulsen HF, Lewis A, Simmons J, Spanos G (eds.) *Proceedings of the 1st international conference on 3D materials science*. Wiley, New York, pp 119–124
- Morawiec A, Glowinski K (2013) On “macroscopic” characterization of mixed grain boundaries. *Acta Mater* 61:5756–5767
- Cahn JW, Taylor JE (2006) Metrics, measures, and parametrizations for grain boundaries: a dialog. *J Mater Sci* 41:7669–7674. doi: [10.1007/s10853-006-0592-8](https://doi.org/10.1007/s10853-006-0592-8)
- Morawiec A (2009) Models of uniformity for grain boundary distributions. *J Appl Cryst* 42:783–792
- Olmsted DL (2009) A new class of metrics for the macroscopic crystallographic space of grain boundaries. *Acta Mater* 57:2793–2799
- Morawiec A (2012) On ‘interface-plane scheme’ and symmetric grain boundaries. *Z Kristallogr* 227:199–206
- Grimmer H (1989) Systematic determination of coincidence orientations for all hexagonal lattices with axial ratio c/a in a given interval. *Acta Cryst A* 45:320–325
- Glowinski K (2013) On frequencies of occurrence of geometrically characteristic grain boundaries. *Sol St Phen* 203–204:427–430
- Patala S, Schuh CA (2013) Symmetries in the representation of grain boundary-plane distributions. *Philos Mag* 93:524–573